Hindawi Publishing Corporation
Mathematical Problems in Engineering
Volume 2013, Article ID 314328, 10 pages
http://dx.doi.org/10.1155/2013/314328

Research Article

Homoclinic Bifurcation and Chaos in a Noise-Induced Φ^6 Potential

Gen Ge,[1] Zhi Wen Zhu,[2] and Jia Xu[2]

[1] *School of Mechanical Engineering, Tianjin Polytechnic University, Tianjin 300160, China*
[2] *School of Mechanical Engineering, Tianjin University, Tianjin 300072, China*

Correspondence should be addressed to Gen Ge; gegenroot@126.com

Received 12 January 2013; Revised 18 April 2013; Accepted 18 April 2013

Academic Editor: Safa Bozkurt Coskun

The present paper focuses on the noise-induced chaos in a Φ^6 oscillator with nonlinear damping. Based on the stochastic Melnikov approach, simple zero points of the stochastic Melnikov integral theoretically mean the necessary condition causing noise-induced chaotic responses in the system. To quantify the noise-induced chaos, the Poincare maps and fractal basin boundaries are constructed to show how the system's motions change from a periodic way to chaos or from random motions to random chaos as the amplitude of the noise increases. Three cases are considered in simulating the system; that is, the system is excited only by the harmonic excitation, by both the harmonic and the Gaussian white noise excitations, or by both the bounded noise and the Gaussian white noise excitations. The results show that chaotic attractor is diffused by the noises. The larger the noise intensity is, the more diffused attractor it results in. And the boundary of the safe basin can also be fractal if the system is excited by the noises. The erosion of the safe basin can be aggravated when the frequency disturbing parameter of the bounded noise or the amplitude of the Gaussian white noise excitation is increased.

1. Introduction

In recent years, stochastic Melnikov method has been applied to study the effects of noise on homoclinic or heteroclinic bifurcation and noise-induced chaos [1–6]. Zhu et al. [7–9] studied a single degree-of-freedom Hamiltonian system subjected to light damping and weakly external and (or) parametric excitations of bounded noise. Xu et al. [10–13] have proposed the effects of bounded noise on the chaotic behavior of the Duffing oscillator under parametric excitation. In the above researches, the random Melnikov process is derived, and a mean-square criterion is used to detect the chaotic motions in the systems. The Melnikov conditions are necessary but not sufficient. Results obtained by the Melnikov approach are therefore weak. Generally, it is not easy to quantify noise-induced chaos, so, as a supplementary method, the numerical simulations are needed. Gan [14, 15] studied the erosion of the boundaries of quadratically system's and double wells system's safe basins. The erosion of the safe basins was found to be aggravated when Gaussian white noise was imposed to the system.

It is known that an important goal of studying dynamical systems is to determine their global structures. Because of the coexistence of period and chaotic attractors, the basin boundaries of attractors are usually fractal and naturally incursive, in the sense that they are related to intersections of stable and unstable manifolds from the saddle points in the system. The intersections of homoclinic orbits or heteroclinic orbits usually mean that chaos arises in the systems. The Poincare maps and fractal basin boundaries are useful tools to study the period or chaotic motions of the single degree-of-freedom systems. In the mentioned researches, Zhu et al. [7–9] and Xu et al. [10–13] used the stochastic Melnikov method and the Poincare maps to show the random chaos of the systems, but in spite of the fact that the chaotic system is sensitive to the initial values, they did not concern the safe basin of the systems to find how the initial conditions influence the system's motion. Gan [14, 15] studied the erosion of the boundaries of the safe basins of a one well system and a double wells system after applying the stochastic Melnikov method. More researches are needed on systems with higher order nonlinear terms which typically lead to more complex

nonlinear characters. Until now, the researchers mentioned previously have studied the response of the system subjected to white noise or bounded noise, but little has been done to find how the white noise and bounded noise influence the systems simultaneously. The joint action of the two kinds of noises can lead to some new dynamical phenomena. So, it is necessary for us to seek for better understanding of the responses of higher order term nonlinear systems with both white noise and bounded noise excitations. In this paper, we consider a triple-well Φ^6 oscillator described by the following equation:

$$\ddot{x} + \omega_0^2 x - \lambda x^2 + \beta x^5 - \left(\mu - \gamma x^2\right)\dot{x} = \xi(t) + f_2 \eta(t). \quad (1)$$

The mathematical model (1) is widely used in vibrating problems. For example, the first-order approximation vibrating models of many beams, bars, and thin plates can be simplified to this form considering the geometric nonlinearity of the structure's deformation. The damping term $(\mu - \gamma x^2)\dot{x}$ in (1) indicates self-excited vibration which is usually caused by the hysteretic nonlinear character of the materials. The exciting terms on the right side of the equation indicate the external forces containing random signals such as wind forces, turbulences, and electromagnetic background noises. So the work in this paper may be helpful for engineers and designers to manufacture the products containing vibrating structures which are subjected to stochastic excitations.

In function (1), λ, β, μ, and γ are constant parameters, $\xi(t)$ is bounded noise and $\eta(t)$ is taken as Gaussian white noise. f_2 is the strength of this stochastic excitation. The bounded noise $\xi(t)$ is a harmonic function with constant amplitude f_1 and random frequency and phase, which can be expressed as:

$$\xi(t) = f_1 \cos(\Omega t + \psi), \quad \psi = \sigma B(t) + \gamma, \quad (2)$$

where Ω, σ, γ, are positive constants; $B(t)$ is unit Wiener process; γ is a random variable uniformly distributed in $[0,2\pi]$. $\xi(t)$ is a stationary random process in wide sense with zero mean. Its covariance is [16]

$$C_\xi(t) = \frac{f_1^2}{2} \exp\left(-\frac{\sigma^2 |\tau|}{2}\right) \cos \Omega t, \quad (3)$$

and its spectral density is (2) as Figure 1 shows:

$$S_\xi(\omega) = \frac{f_1^2 \sigma^2}{2\pi} \left(\frac{1}{4(\omega - \Omega)^2 + \sigma^4} + \frac{1}{4(\omega - \Omega)^2 + \sigma^4}\right). \quad (4)$$

The variance of the bounded noise is

$$C_\xi(0) = \frac{f_1^2}{2}. \quad (5)$$

The position of the peak of the spectral density depends on Ω, and the bandwidth of the noise depends mainly on σ. It is a narrow-band process when σ is small. The spectrum density for the Gaussian white noise $\eta(t)$ is assumed to be S_0 with the strength $D\,(= 2\pi S_0)$. It can be shown that the functions of the noise are continuous and bounded, which are required in the derivation of Melnikov function.

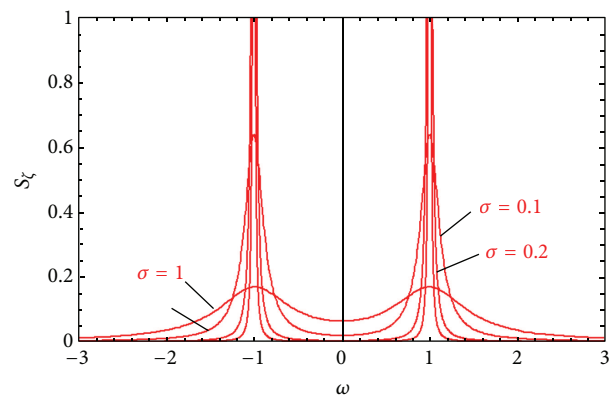

Figure 1: The spectral densities of bounded noise.

2. The Undisturbed System

In the following discussion, the parameters of system (2) are fixed as $\omega_0 = 1$, $\lambda = 0.5$, $\beta = 0.052$, $\Omega = 1$, and the strength of the white noise $D = 1$. The corresponding Hamiltonian (unperturbed system) can be obtained by introducing two state variables q and p:

$$\begin{aligned} \dot{q} &= p, \\ \dot{p} &= -\omega_0^2 q + \lambda q^2 - \beta q^5 \end{aligned} \quad (6)$$

with Hamilton function

$$H(q,p) = \frac{1}{2}p^2 + \frac{1}{2}\omega_0^2 q^2 - \frac{1}{4}\lambda q^4 + \frac{1}{6}\beta q^6. \quad (7)$$

When $\lambda^2 > 4\beta\omega_0^2$, through the analysis of the fixed points (q_i, p_i) and their stability for (2), one can see that there exist five fixed points: $(+q_1, -q_1)$ being saddles, $(+q_2, 0, -q_2)$ being centers, as shown in Figure 1, where

$$\begin{aligned} \pm q_1 &= \pm\sqrt{\frac{\lambda}{2\beta} - \frac{\sqrt{\lambda^2 - 4\beta\omega_0^2}}{2\beta}}, \\ \pm q_2 &= \pm\sqrt{\frac{\lambda}{2\beta} + \frac{\sqrt{\lambda^2 - 4\beta\omega_0^2}}{2\beta}}. \end{aligned} \quad (8)$$

There is a homoclinic orbit Γ_{ho}^+ to and from $+q_1$ and another homoclinic orbit Γ_{ho}^- to and from $-q_1$. And there is a heteroclinic orbit Γ_{he}^+ from $+q_1$ to $-q_1$, together with another heteroclinic orbit Γ_{he}^- from $-q_1$ to $+q_1$. The phase portrait and the potential function of system (6) are shown in Figures 2(a) and 2(b), respectively. That is to say, the system has two hyperbolic fixed points, and each point processes two different types of orbits: a symmetric pair of homoclinic trajectories connected each point to itself given by

$$\begin{aligned} q_0 &= \pm\frac{\sqrt{2} q_1 \cosh(\kappa t/2)}{\sqrt{\alpha + \cosh(\kappa t)}}, \\ p_0 &= \pm\frac{\sqrt{2} q_1 T (1 - \alpha) \sinh(\kappa t/2)}{2[\alpha + \cosh(\kappa t)]^{3/2}}, \end{aligned} \quad (9)$$

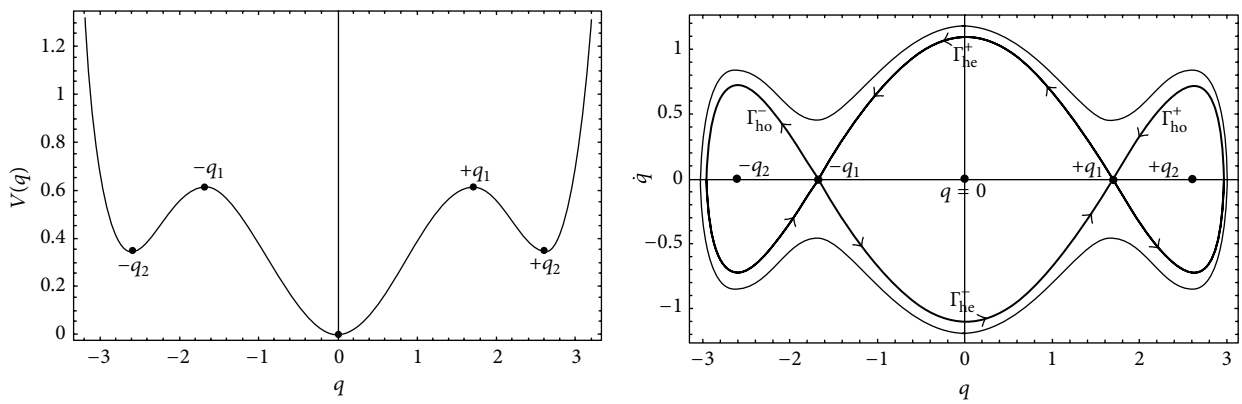

(a) (b)

Figure 2: Phase portrait and potential of system (1).

and a heteroclinic orbit connecting the saddle points defined as

$$q_0 = \pm \frac{\sqrt{2} q_1 \sinh(\kappa t/2)}{\sqrt{-\alpha + \cosh(\kappa t)}},$$
$$p_0 = \pm \frac{\sqrt{2} q_1 T (1-\alpha) \cosh(\kappa t/2)}{2[-\alpha + \cosh(\kappa t)]^{3/2}}, \tag{10}$$

where

$$\kappa = q_1^2 \sqrt{2\beta(\theta - 1)}, \qquad \alpha = \frac{5 - 3\theta}{3\theta - 1},$$
$$\theta = \frac{-\lambda - \sqrt{\lambda^2 - 4\beta\omega_0^2}}{-\lambda + \sqrt{\lambda^2 - 4\beta\omega_0^2}}. \tag{11}$$

3. Homoclinic Bifurcation and Chaos for Noise Free Condition

For the condition $\psi = 0, f_2 = 0$, the system (1) is deterministic. Now, suppose that μ, γ, and f are small parameters with the same order as ε, denoted as $\mu = \varepsilon\mu$, $\gamma = \varepsilon\gamma$, and $f = \varepsilon f$. The homoclinic or heteroclinic orbits of the unperturbed system (6) are expressed as (8) and (9). The Melnikov function is expressed as

$$M(t_0) = -\int_{-\infty}^{+\infty} \left(\mu - \gamma q_0^2\right) p_0^2 dt + \int_{-\infty}^{+\infty} f p_0 \cos\left[\Omega(t + t_0)\right] dt. \tag{12}$$

Substituting (8), (9) into (12), we get

$$\begin{aligned} M(t_0) = {} & \Bigg(\kappa\mu \Bigg[(2+\alpha)\sqrt{1-\alpha^2} + (2+4\alpha) \\ & \times \operatorname{ArcTan}\left(\frac{-1+\alpha}{\sqrt{1-\alpha^2}}\right)\Bigg] q_1^2\Bigg) \\ & \times \left(4\sqrt{1-\alpha}(1+\alpha)^{3/2}\right)^{-1} \\ & - \Bigg((-1+\alpha)^2 \kappa\gamma \\ & \times \Bigg[\sqrt{1-\alpha^2}\left(2+\alpha^2\right) \\ & + 6\delta \operatorname{ArcTan}\left(\frac{-1+\alpha}{\sqrt{1-\alpha^2}}\right)\Bigg] q_1^4\Bigg) \\ & \times \left(12\left(1-\alpha^2\right)^{5/2}\right)^{-1} \\ & + 2 f q_1 \sin\left[\frac{2}{T}\right] \sin\left[t_0\right]. \end{aligned} \tag{13}$$

When $M(t_0) = 0$, the threshold value f_1 leading to homoclinic bifurcation is obtained.

Basin boundary simulations are one means for checking homoclinic or heteroclinic bifurcation. The result of Thothadri and Moon [17] implies that a homoclinic or heteroclinic bifurcation is a sufficient condition for the appearance of fractal basin boundaries. Such fractal boundaries indicate whether the system is attracted to one or another periodic attractor. In this condition, the system may be very sensitive to initial conditions. Thus, small uncertainties in the initial conditions can lead to unpredictability of the system output even if the motion is not chaotic.

Numerical simulations are carried out in order to determine the basin's boundaries of the noise-free system (1) for different values of the harmonic excitation amplitude f_1. The steady-state motion will be periodic around the attractors near the fixed points $(-q_2, +q_2)$ when f_1 is small. Even if

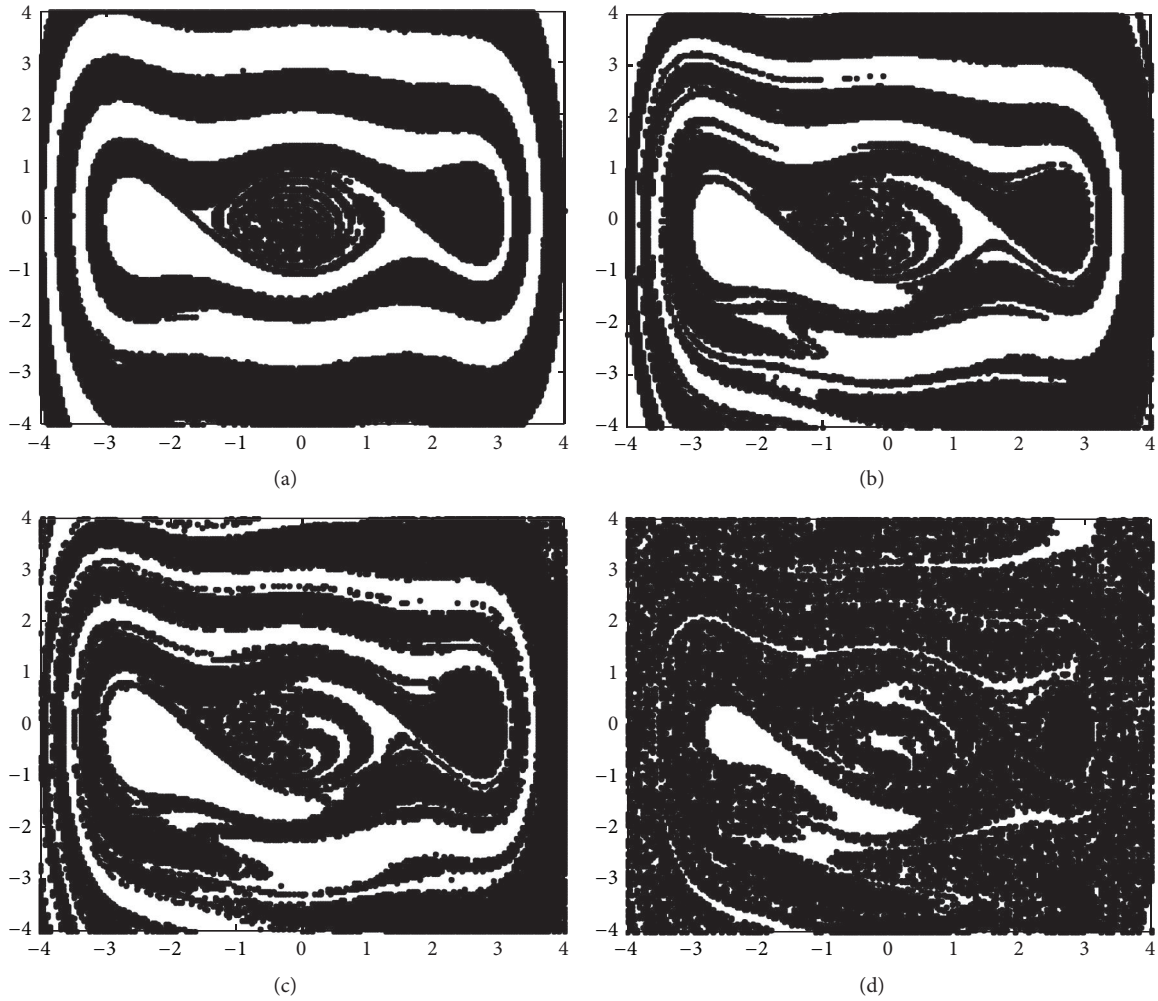

FIGURE 3: Basins of attraction for motion around $q = +q_2$: (a) $f_1 = 0.05$, (b) $f_1 = 0.15$, (c) $f_1 = 0.19$, and (d) $f_1 = 0.30$.

f_1 is increased beyond the critical value for homoclinic bifurcation, the final steady motion will still possible be periodic rather than chaotic. Note that the results of Figure 3 represent the basins of attraction of the motion around the well $q = +q_2$. And Figure 4 corresponds to the basins of attraction of the motion around the well $q = -q_2$ with the same harmonic excitation values f_1. By scanning the initial values in the (q, p) plane for various values of f_1, we can observe that when f_1 is less than the homoclinic threshold value $f_1 = 0.096$, the boundary of the basins of attraction (marked regions) is regular (see Figures 3(a) and 4(a)), As f_1 increases, the regular boundary of basin of attraction is destroyed and the fractal shape becomes more and more visible (see Figures 3(b)–3(d) and Figures 4(b)–4(d)).

Melnikov conditions are necessary but not sufficient leading to chaos. Results obtained by the Melnikov method are therefore weak. By some numerical simulations, the threshold value f_1 rising chaos equals 0.48 which is larger than $f_1 = 0.096$ yielded by (13). The numerical results are shown in Figure 5. As one sees, Figures 5(a) and 5(b) are the time series and the phase portraits. The Poincare maps shown in Figure 5(c) with beautiful fatal shape and the spectrum shown in Figure 5(d) with multipeaks all indicate that the system is chaotic. Furthermore, it is necessary to explore the situation that the system is exhibited by bounded noise and Gaussian white noise, respectively. In the following section, the condition $\psi \neq 0$, $f_2 \neq 0$ is considered.

4. The Random Melnikov Process

Melnikov process can be used here since a bounded noise with spectral density of (4) can be approximated by a sum of many harmonic functions with different frequencies and random phases. The random Melnikov process can be obtained by using the formula given by Wiggins [18]:

$$\begin{aligned} M(t_1, t_2) &= -\int_{-\infty}^{+\infty} \left(\mu - \gamma q_0^2\right) p_0^2 dt + \int_{-\infty}^{+\infty} f_1 p_0 \xi(t - t_1)\, dt \\ &\quad + \int_{-\infty}^{+\infty} f_2 p_0 \eta(t - t_2)\, dt \\ &= -T + Z_1(t_1) + Z_2(t_2), \end{aligned} \tag{14}$$

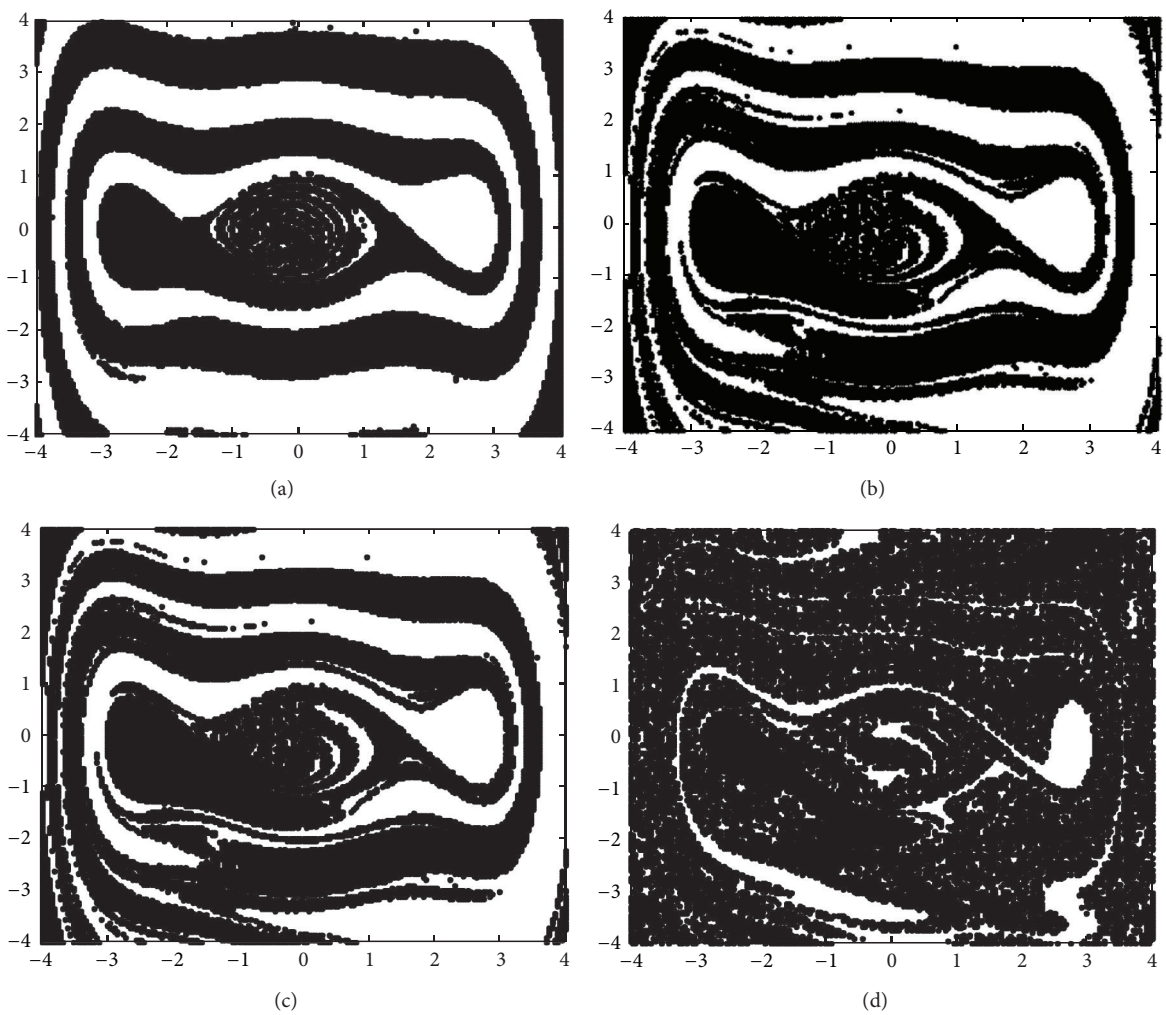

Figure 4: Basins of attraction for motion around $q = -q_2$: (a) $f_1 = 0.05$, (b) $f_1 = 0.15$, (c) $f_1 = 0.19$, and (d) $f_1 = 0.30$.

where the first integral represents the mean of the random Melnikov process due to the nonlinear damping, and the last two integrals denote the random portion due to random excitations. The expression $h_i(t) = f_i p_0(t)$ $(i = 1, 2)$ can be regarded as the impulse response function of an invariant linear system while $\xi(t)\,\eta(t)$ are inputs of the system. Thus, the variance of Z_i $(i = 1, 2)$ as the output of the system can be obtained:

$$\sigma_{z1}^2 = \int_{-\infty}^{+\infty} \left|H_1(\omega)\right|^2 S_\xi(\omega)\, d\omega,$$
$$\sigma_{z1}^2 = \int_{-\infty}^{+\infty} \left|H_2(\omega)\right|^2 S_0 d\omega, \tag{15}$$

where $S_\xi(\omega)$ is the spectral density of $\xi(t)$, S_0 is the spectral density of Gaussian white noise process $\eta(t)$, and $H_i(\omega)$ is the frequency response function of the system obtained through Fourier transform

$$H_i(\omega) = \int_{-\infty}^{+\infty} f_i p_0 e^{-i\omega t} dt \quad (i = 1, 2). \tag{16}$$

Since p_0 is an odd function of time for the homoclinic orbit, the criterion for possible chaotic motion based on Melnikov process is performed in mean-square representation:

$$\begin{aligned}
&\left\langle \int_0^{+\infty} (\mu - \gamma q_0^2) p_0^2 dt \right\rangle^2 \\
&\quad \le {f_1}^2 \int_0^{+\infty} \left| \int_0^{+\infty} p_0 \sin \omega t\, dt \right|^2 \frac{\sigma^2}{\pi} \\
&\qquad \times \left(\frac{1}{4(\omega - \Omega)^2 + \sigma^4} + \frac{1}{4(\omega + \Omega)^2 + \sigma^4} \right) d\omega \\
&\qquad + f_2^2 \int_0^{+\infty} \left| \int_0^{+\infty} p_0 \sin \omega t\, dt \right|^2 S_0 d\omega.
\end{aligned} \tag{17}$$

Inequality (17) tells that the chaotic response may be induced by the bounded noise and Gaussian white noise excitation simultaneously. Moreover, we should note that inequality (17) is not sufficient, and other measures are needed for identification of the system's chaotic response. In

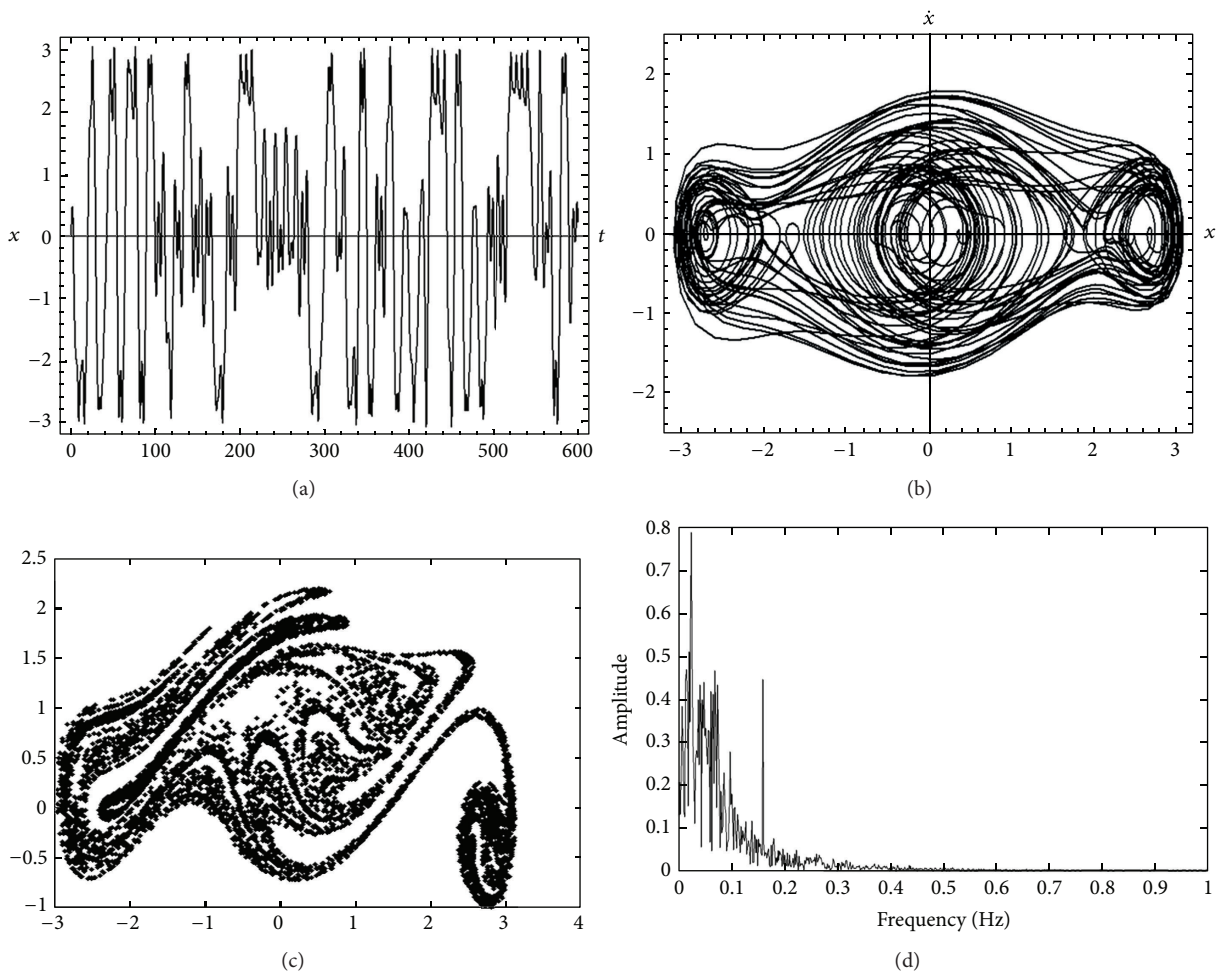

Figure 5: Chaos for the noise system with $f_1 = 0.49$: (a) time series, (b) phase portraits, (c) poincare maps, (d) spectrum.

the following, the Poincare maps and the fractal boundary of safe basin of the system are presented respectively.

5. Poincare Maps

It is as well known that Poincare maps are useful tools to characterize the dynamics of system quantitatively. Hence we investigate system (1) through its Poincare maps. The successive iteration of Poincare map is defined as

$$P : \Sigma \longrightarrow \Sigma, \quad \Sigma = \left\{ (x(t), \dot{x}(t)) \mid t = 0, \frac{2\pi}{\Omega}, \frac{4\pi}{\Omega}, \ldots \right\} \in R^2. \tag{18}$$

The system is solved by the Rutter-Kutter method, and the solution is plotted for every $t = 2\pi/\Omega$. Totally, 10000 periods are calculated with 200 points each time period; the first 20000 points are deleted, and the following iteration points are plotted. One can see from Figure 6 that the chaotic attractor is diffused by the noises, and the larger noise intensity results in the more diffused attractor. The amplitude of the bounded noise is set as $f_1 = 0.49$.

In Figures 6(a)–6(d), one can see when system (1) is only excited by the bounded noise, the fractal shape of the Poincare map will be destroyed with the increasing of the frequency disturbing parameter σ from 0.01 to 0.5. And the area of the chaotic attractor in the phase plane is becoming larger because of the diffusing caused by the bounded noise. On the other hand, when system (1) is excited by harmonica excitation ($\sigma = 0$) and the Gaussian white noise, respectively, the chaotic attractor is diffused by the white noises too. From Figures 6(e)–6(f), it is obvious that the area of the chaotic attractor is decreased with the increase of the exciting intensity f_2 from 0.2 to 0.35.

6. Basin Erosion

The decrease of safe basins area is often called basin erosion. Since those intersections of stable and unstable manifolds map one to another, the manifolds present a convoluted structure that extends through a wide region of the phase space. The transient orbits near such a fractal basin boundary will be as convoluted as the boundary itself. So they are expected to cross the critical line very often, increasing dramatically the number of unsafe initial conditions [14]. In the view of this point, the erosion of the safe basin is usually related to fractal basin boundary of attractors. The

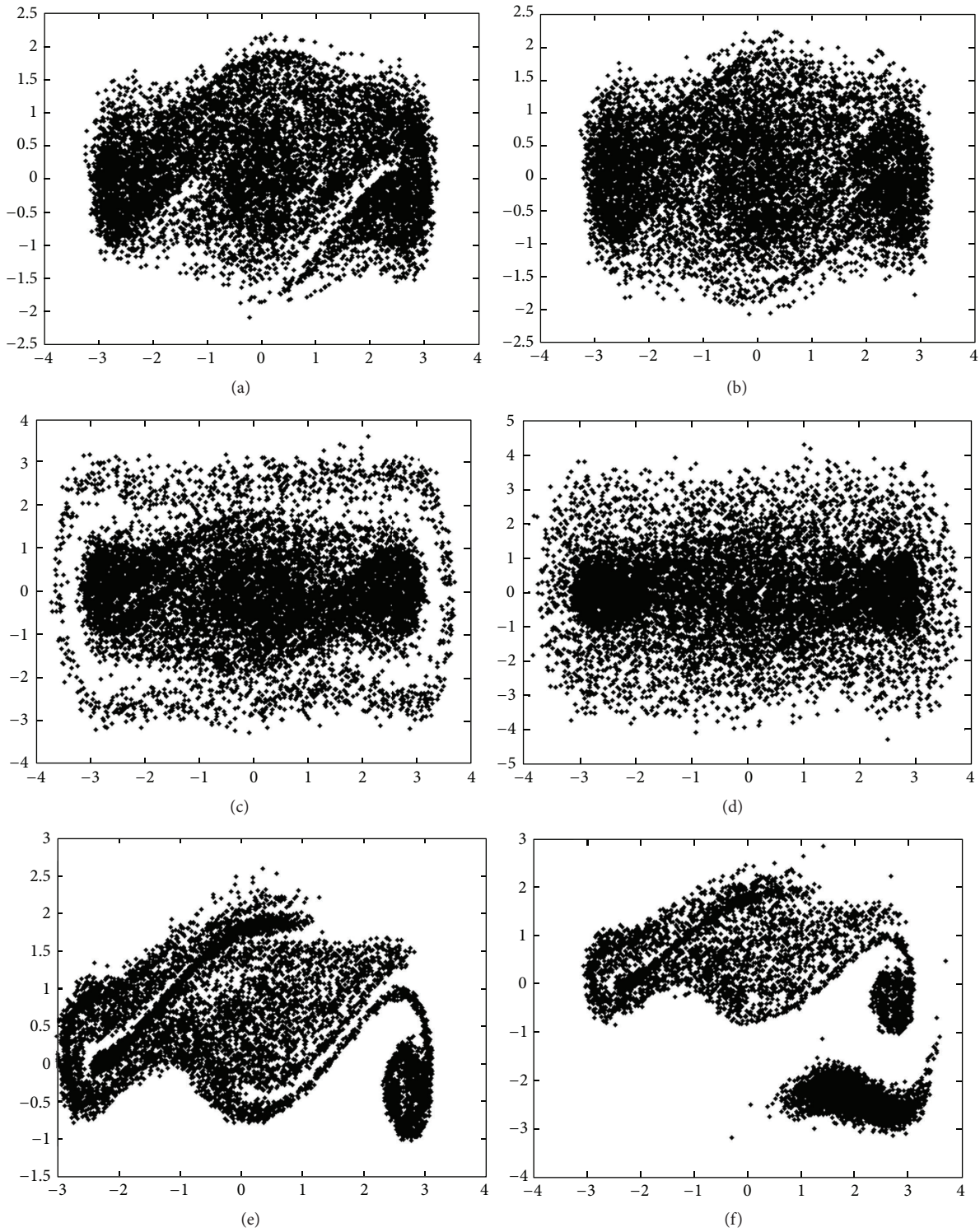

Figure 6: Poincare map for noisy system with (a) $f_1 = 0.49$, $\sigma = 0.01$, and $f_2 = 0$; (b) $f_1 = 0.49$, $\sigma = 0.05$, and $f_2 = 0$; (c) $f_1 = 0.49$, $\sigma = 0.1$, and $f_2 = 0$; (d) $f_1 = 0.49$, $\sigma = 0.5$, and $f_2 = 0$; (e) $f_1 = 0.49$, $\sigma = 0$, and $f_2 = 0.2$; (f) $f_1 = 0.49$, $\sigma = 0$, and $f_2 = 0.35$.

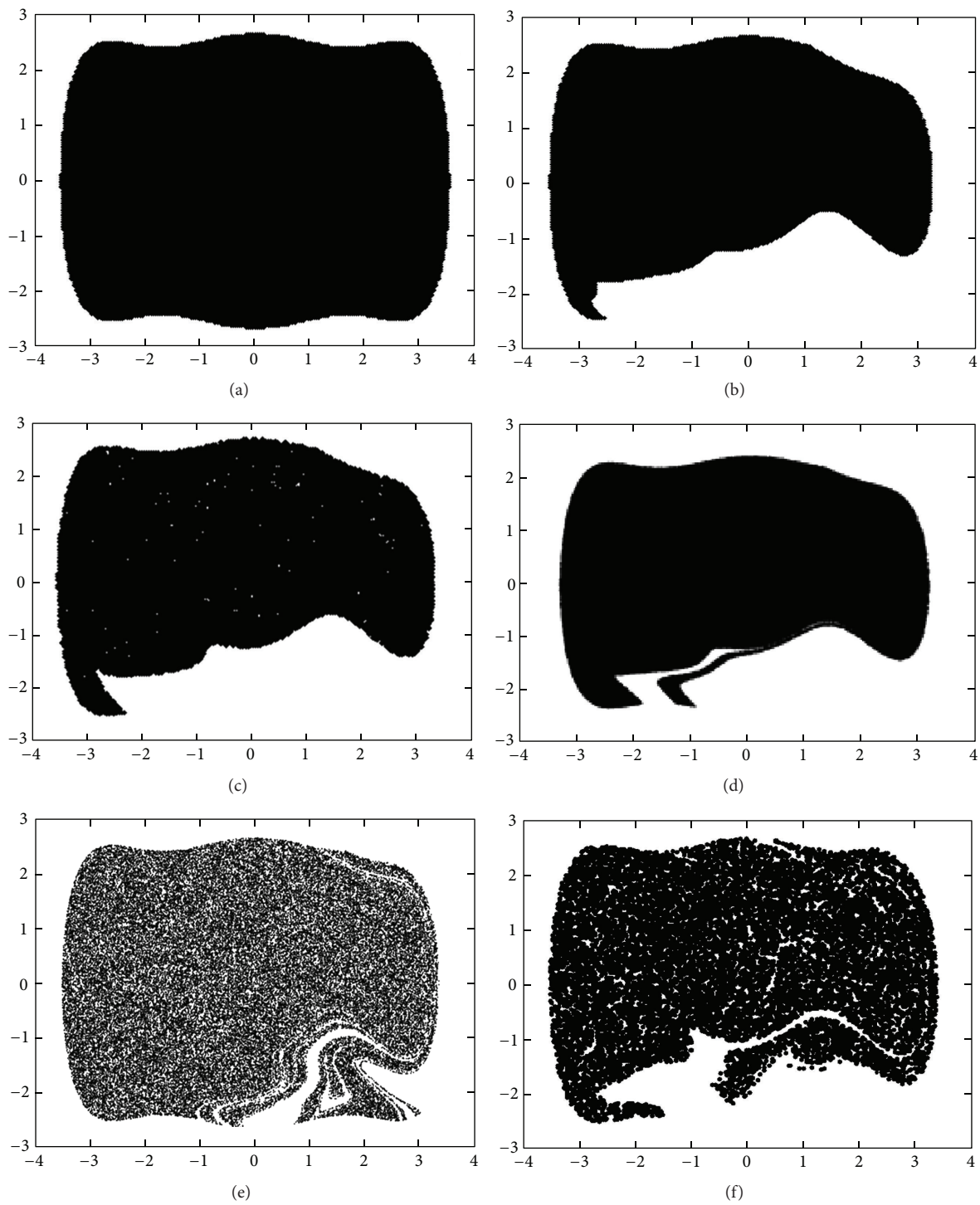

Figure 7: The boundary of safe basin (a) $f_1 = 0$, f_2=0; (b) $f_1 = 0.49$, $\sigma = 0$, and $f_2 = 0$; (c) $f_1 = 0.49$, $\sigma = 0.1$, and $f_2 = 0$; (d) $f_1 = 0.49$, $\sigma = 0.145$, and $f_2 = 0$; (e) $f_1 = 0.49$, $\sigma = 0$, and $f_2 = 0.7$; (f) f_1= 0.49, $\sigma = 0.145$, and $f_2 = 0.7$.

safe basin without erosion is drawn within the region G surrounded by the coincident stable and unstable manifolds of the conservative case of system (1) with $f_1 = f_2 = \mu = \gamma = 0$ (see Figure 7(a)), which is defined by

$$G = \left\{(x, y) \mid -\sqrt{2\left(H - \frac{1}{2}x^2 + \frac{1}{4}\lambda x^4 - \frac{1}{6}\beta x^6\right)} \le y \le \sqrt{2\left(H - \frac{1}{2}x^2 + \frac{1}{4}\lambda x^4 - \frac{1}{6}\beta x^6\right)}\right\} \in R^2. \tag{19}$$

When the Hamiltonian value of any phase point $(x(t), y(t))$ of the systems trajectory is larger than H within 100 thousand steps, this motion initiating from the

corresponding initial point is considered to be unsafe and this initial point is discarded.

In Figure 7(a) (in which H is set to 3.5), the safe basin is a closed and apparently smooth curve when $f_1 = f_2 = 0$. Following the increase of the driving amplitude f_1, this orbit will undergo a bifurcation leading to chaos, and the boundary of the safe basin is shown to be fractal (see Figure 7(b)). In general, the area of the safe basin decreases following the decrease of the Hamiltonian H.

To learn the effect of the noise excitation of the erosion of safe basin, the system is excited by the bounded noise and white noise. In Figure 7(c), it is clear that the boundary of safe basin will not change when the frequency disturbing parameter σ is small enough. When the frequency disturbing parameter σ exceeds 0.14, the boundary of the safe basin is shown to be more fractal (see Figure 7(d)). Figures 7(e) and 7(f) present a sequence of safe basins when the Gaussian white noise is added to the system. The inclusively fractal fingers are also observed, which means that chaotic responses still exist in the stochastic case of system (1).

7. Discussion

From the numerical results presented in Section 5, the Poincare maps show that the chaotic attractor is diffused by the bounded noises, and the larger the noise intensity is, the more diffused attractor it results in. Similar results can be found in Zhu et al's [7–9] and Xu et al.'s [10–13] researches. But results are different when the system is excited by Gaussian white noise. The chaotic attractor has a similar pattern of structure to the deterministic case with weak white noise excitation (see Figures 6(e) and 5(c)). As the Gaussian white noise is considerably strong, the structure of the chaotic attractor will be changed (see Figure 6(f)). However, the increasing Gaussian white noise excitation does not seem to result in more diffused attractor. On the contrary, the size of the chaotic attractor is reduced by increasing the white noise.

The effect of noise on the boundary of the safe basin is also discussed by the numerical results presented in Section 6. The erosion can be aggravated when the frequency disturbing parameter of the bounded noise or the amplitude of the Gaussian white noise excitation is increased (see Figures 7(d) and 7(e)). Similar results can also be found in Gan's [14, 15] works. When the system is excited by Gaussian white noise combined with bounded noise, one can find that the boundary of the safe basin does not seem to be more fractal. Comparing Figure 7(e) with Figure 7(f), the author prefers to describe the safe basin in Figure 7(f) as "random" rather than "fractal" for some points that are deleted randomly in the safe basin, and the fractal boundaries are almost destroyed. From the previous results, it is found that the frequency disturbing parameter of the bounded noise is more likely to affect the inner part of the safe basin while the Gaussian white noise may have more influences on the safe basin's boundaries.

We can explain the phenomena above like this: when the Gaussian white noise excitation is imposed on the system, the closed loops of the stable and the unstable manifolds in the corresponding undisturbed system can also be broken, but they will intersect randomly with each other, which thus causes the basin erosion. The changing of frequency disturbing parameter does not affect the amplitude of the bounded noise which is the main cause of the disturbing to the system.

8. Conclusion

The present paper demonstrates the effects of the bounded noise and Gaussian white noise on Poincare maps and the boundary of the safe basin, respectively, in the triple-well Φ^6 potential nonlinear oscillator. Firstly, the noise free system is discussed using the Melnikov method and numerical simulation. The results show that although the Homoclinic bifurcation condition is satisfied, the response of the system nevertheless undergoes harmonic motions rather than chaotic motions. Furthermore, the fractal basin boundaries can be observed. By applying the stochastic Melnikov approach, the necessary condition for the arising of chaos is obtained, from which one can know that the chaotic and the thoroughly random responses can exist in the system, even though the stochastic Melnikov condition is satisfied. The numerical simulation illustrates that the noises affect the size of the chaotic attractor in the Poincare maps and the erosion of the safe basin. The bounded noise is more likely to diffuse the attractor while the white noise is prone to decrease the size of the attractor. At last, the simulation of the safe basin indicates that the strength of the white noise is more likely to cause fractal boundaries than the frequency disturbing parameter of the bounded noise.

However, the chaotic system induced by the noise has many complex and interesting phenomena which cannot be explained rigorously by theories. Therefore, more further researches are needed.

Acknowledgments

This work was supported by the National Natural Science Foundation of China (Grant no. 11272229) and Science Foundation of Tianjin Education Committee (Grant no. 20120902).

References

[1] A. R. Bulsara, W. C. Schieve, and E. W. Jacobs, "Homoclinic chaos in systems perturbed by weak Langevin noise," *Physical Review A*, vol. 41, no. 2, pp. 668–681, 1990.

[2] M. Frey and E. Simiu, "Equivalence between motions with noise-induced jumps and chaos with smale horseshoes," in *Proceedings of the 9th Conference on Engineering Mechanics (ASCE '92)*, pp. 660–663, May 1992.

[3] M. Frey and E. Simiu, "Noise-induced chaos and phase space flux," *Physica D*, vol. 63, no. 3-4, pp. 321–340, 1993.

[4] W. C. . Xie, "Effect of noise on chaotic motion of buckled column under periodic excitation," *Nonlinear and Stochastic Dynamics*, vol. 78, pp. 215–225, 1994.

[5] E. Simiu and M. R. Frey, "Melnikov processes and noise-induced exits from a well," *Journal of Engineering Mechanics*, vol. 122, no. 3, pp. 263–270, 1996.

[6] H. Lin and S. C. S. Yim, "Analysis of a nonlinear system exhibiting chaotic noisy chaotic and random behaviors," *ASME Journal of Applied Mechanics*, vol. 63, no. 2, pp. 509–516, 1996.

[7] Z. H. Liu and W. Q. Zhu, "Homoclinic bifurcation and chaos in simple pendulum under bounded noise excitation," *Chaos, Solitons and Fractals*, vol. 20, no. 3, pp. 593–607, 2004.

[8] W. Y. Liu, W. Q. Zhu, and Z. L. Huang, "Effect of bounded noise on chaotic motion of duffing oscillator under parametric excitation," *Chaos, Solitons and Fractals*, vol. 12, no. 3, pp. 527–537, 2001.

[9] Z. H. Liu and W. Q. Zhu, "Homoclinic bifurcation and chaos in coupled simple pendulum and harmonic oscillator under bounded noise excitation," *International Journal of Bifurcation and Chaos in Applied Sciences and Engineering*, vol. 15, no. 1, pp. 233–243, 2005.

[10] Z. Sun, W. Xu, and X. Yang, "Effect of random noise on chaotic motion of a particle in a Φ^6 potential," *Chaos, Solitons and Fractals*, vol. 27, no. 1, pp. 127–138, 2006.

[11] X. Yang, W. Xu, Z. Sun, and T. Fang, "Effect of bounded noise on chaotic motion of a triple-well potential system," *Chaos, Solitons and Fractals*, vol. 25, no. 2, pp. 415–424, 2005.

[12] X. Yang, W. Xu, and Z. Sun, "Effect of bounded noise on the chaotic motion of a Duffing Van der pol oscillator in a Φ^6 potential," *Chaos, Solitons and Fractals*, vol. 27, no. 3, pp. 778–788, 2006.

[13] J. Li, W. Xu, X. Yang, and Z. Sun, "Chaotic motion of Van der Pol-Mathieu-Duffing system under bounded noise parametric excitation," *Journal of Sound and Vibration*, vol. 309, no. 1-2, pp. 330–337, 2008.

[14] C. Gan, "Noise-induced chaos in a quadratically nonlinear oscillator," *Chaos, Solitons and Fractals*, vol. 30, no. 4, pp. 920–929, 2006.

[15] C. Gan, "Noise-induced chaos in duffing oscillator with double wells," *Nonlinear Dynamics*, vol. 45, no. 3-4, pp. 305–317, 2006.

[16] Y. K. Lin and G. Q. Cai, *Probabilistic Structural Dynamics: Advanced Theory and Applications*, McGraw-Hill, New York, NY, USA, 1995.

[17] M. Thothadri and F. C. Moon, "Nonlinear system identification of systems with periodic limit-cycle response," *Nonlinear Dynamics*, vol. 39, no. 1-2, pp. 63–77, 2005.

[18] S. Wiggins, *Global Bifurcations and Chaos: Analytical Methods* , Springer, New York, NY, USA, 1988.